Building up Nanotubes: Docking of "Janus" Cyclodextrins in Solution

Javier Rodriguez,[†] Rocío Semino, and Daniel Laria*

Departamento de Física de la Materia Condensada, Comisión Nacional de Energía Atómica, Av. Gral. Paz 1499, (1650) San Martín, Prov. de Buenos Aires, Argentina, and Facultad de Ciencias Exactas y Naturales, Departamento de Química Inorgánica Analítica y Química e INQUIMAE, Pabellón II, Ciudad Universitaria, (1428) Capital Federal, Argentina

Using molecular dynamics experiments, we analyze the association of "Janus" 6-amino-6-deoxy-2O-carboxymethyl-β-cyclodextrins (JCD) in aqueous solutions. In JCD dimers, the free energy associated with the primary-rim−secondary-rim docking shows a stable minimum of ~-45 kcal mol^{-1}. Trimers in solution are also remarkably stable, exhibiting minimal distortions in their spatial and orientational distributions. The resulting geometrical docking shows the incipient characteristics of flexible nanotubes in solution, with eventual water interchange between the central channel and the bulk at the junctions between monomers. Structural and dynamical properties of the trapped water filling the nanotube are dictated to a large exent by the charge density at the rims.

Cyclodextrins (CD) represent versatile complexation agents in solution.[1] Most of their distinctive characteristics derive from their overall molecular shape, normally portrayed in terms of a cylindrical hydrophobic cavity connecting two hydroxylated, primary (PR) and secondary (SR), rims (see Figure 1). In this Letter, we will focus attention on "Janus" cyclodextrins (JCD), that is, functionalized oligosaccharides[2−5] exhibiting charge localization of opposite signs at these two rims. In a recent article, the synthesis of 6-amino-6-deoxy-2-*O*-carboxymethyl-β-CD in aqueous solution has been reported.[6] Results from transmission electron microscopy experiments suggest that, at neutral pH, they may self-assemble, in a face-to-face geometrical arrangement, giving rise to flexible ribbons in solutions. As such, the resulting structures would be akin to those reported for charged CD heterodimers[2] and nanotubes synthesized from ring peptides with alternating D- and L-amino acids as well.[7] In what follows, we will present results from molecular dynamics experiments that bring support to the latter hypothesis. Our main objective was to elucidate microscopic characteristics pertaining to the stability and solvation of JCD dimers and trimers in aqueous solutions.

The simulated systems were fully periodic; they were composed of two and three JCDs immersed in a box with linear dimensions of 30 Å × 30 Å × 60 Å, containing $N_w = 1654$ water molecules. The NAMD code,[8] with the force field corresponding to the CHARMM22 parametrization,[9] was used to run the dynamics of the systems. Interactions involving water molecules were modeled using the classical TIP3P Hamiltonian.[10] All trajectories corresponded to *NPT* runs and were generated by implementing Langevin dynamics at $T = 298$ K and $p = 1$ bar. Meaningful statistics were collected along three uncorrelated runs, each one lasting 4 ns. Long-ranged Coulomb
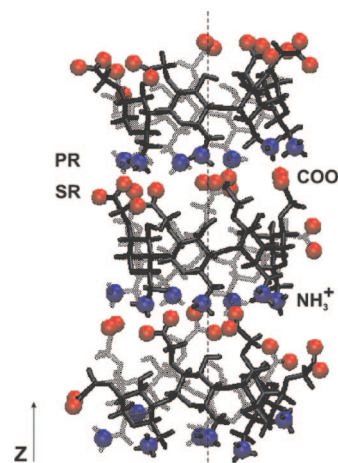
* To whom correspondence should be addressed. E-mail: dhlaria@cnea.gov.ar.
† E-mail: javier@speedy.cnea.gov.ar.

Figure 1. Snapshot of the JCD trimer exhibiting the sequence of two PR−SR dockings (see text).

interactions were treated using Ewald sums, implemented by a particle mesh procedure.[11,12]

Site coordinates of the JCD were obtained from X-ray information for nonfunctionalized β-CD.[13] This initial geometrical arrangement and the partial charges provided by CHARMM2 parametrization yield a dipole moment for the JCD monomer on the order of $\mu_{JCD} \sim 200$ D. Initial configurations were obtained by approaching the primary and secondary rims of two JCDs in vacuo, with their dipolar moments aligned in a parallel fashion along the *z*-axis of the simulation box. The initial distance between centers of mass of adjacent JCDs was set to $\Delta z_{CM} \sim 12$ Å. The simulation box was filled up with water molecules and equilibrated along a $\sim$300 ps run, during which only the solvent molecules were allowed to move, at temperatures close to $T = 700$ K. From then on, the systems were gradually cooled down to ambient conditions by multiple rescalings of the atomic velocities during the subsequent 300
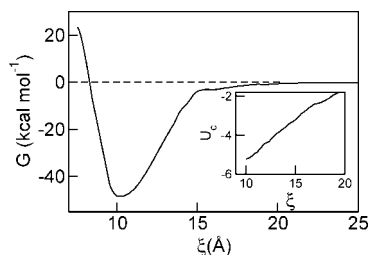
Figure 2. Free energy associated with the dimerization of a JCD pair in aqueous solution. The inset shows results for the Coulomb intermolecular coupling between the JCD pair in solution (the units of the y-axis correspond 10^2 kcal mol^{-1}).
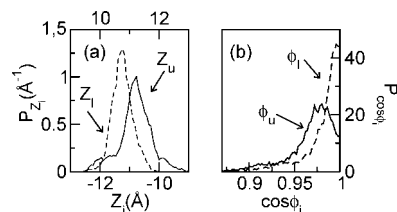

Figure 3. Panel (a): Distribution function for the z-component of the vector separating the centers of mass of adjacent JCDs (Z_l: lower x-axis; Z_u: upper x-axis). Panel (b): Same as panel (a) for relative orientations.

ps. Following this initial thermalization period, all constraints on the JCDs were released and replaced by seven soft harmonic interactions ($k_{hrm} \sim 15$ kcal mole^{-1} Å^{-2}) acting on each glycosidic oxygen site of one JCD (the central one, for the trimer case), centered at the corresponding initial positions. This procedure has been implemented in the past in similar simulation experiments[14−16] and helps to preserve the initial orientation of the tagged JCD with respect to the rectangular simulation box axes, introducing negligible effects on the dynamics of the system.

We will start our analysis by examining the stability of the PR−SR docking of the JCD dimer in aqueous solution. The computation of the dimerization free energy requires harvesting of fluctuations over phase space regions which may eventually include different docking arrangements between monomers. Yet, on the basis of an educated guess, we tend to believe that the most relevant fluctuations are captured by $G(\xi)$, the free energy associated with the geometrical order parameter ξ describing the association process along a collinear docking channel.

$$-\beta G(\xi°) \propto \ln\langle\delta(\xi - \xi°)\rangle \tag{1}$$

In the previous expression, the angular brackets denote an equilibrium ensemble average and $\beta^{-1} = k_B T$ represents the Boltzmann constant times the temperature. Our definition for the order parameter is $\xi = |Z^1_{JCD} - Z^2_{JCD}|$, where Z^i_{JCD} ($i = 1, 2$) corresponds to the z-coordinate of the center of mass of the ith JCD. A plot of the dimerization free energy, obtained from the implementation of an adaptive biasing forces (ABF) scheme,[17−19] is shown in Figure 2. Briefly, this methodology relies on the generation of trajectories along a chosen reaction coordinate, experiencing practically no free-energy barriers. This is achieved by means of biasing forces estimated along a series of small bins which, in turn, span the complete ξ interval. Very recently, ABF schemes have been successfully employed in analyses of CD encapsulation of complex guest molecules, such as cholesterol[15] or rotaxane.[16]

The profile of Figure 2 presents a -46.2 kcal mol^{-1} single minimum at $\xi_0 = 10.1$ Å and no structure beyond $\xi \gtrsim 15$ Å. The magnitude of the minimum should be compared with estimates for association free energies between ionic heterodimers and nonfunctionalized CD in solution,[2,20] $\Delta G \sim 10-15$ kcal mol^{-1}. Contrasting with the usual free energy associated with the pairing of simple ions in solution,[21,22] the curve shows practically no signs of marginally stable solvent-separated JCD pairs. In fact, this is not totally unexpected since a given value of ξ is likely to be associated with a wide variety of similar $-COO^-\cdots H_2O\cdots {}^+H_3N-$ distances. As such, thermal fluctuations should necessarily wash out any structure beyond the global minimum.

Effects from the solvent reactive field on the dimerization process can be estimated by comparing the $G(\xi)$ curve with that obtained from averages of the intermolecular Coulomb coupling $U_c(\xi)$ between the JCD pair in solution (see inset of Figure 2). Note that solvation reduces the reversible work to dissociate the JCD pair in a sensible fashion, becoming 1 order of magnitude smaller than the prediction based on the magnitude of $U_c(\xi_0) \sim -560$ kcal mol^{-1}.

The role of the solvent is not exclusively restricted to provide the usual dielectric screening of intermolecular Coulomb interactions. In fact, solvation is also a key ingredient that determines the resulting overall intramolecular structure of the JCD monomers in solution and, in turn, the characteristics of the dimer docking. We note that, even in the JCD monomer in vacuo, strong Coulomb interactions between terminal charged groups lead to twists, most notably in the secondary O-2 carboxymethyl chains and in the $\alpha(1-4)$ glycosidic linkages, which significantly distort the toroidal shape usually found in CDs. The presence of a polar environment partially shields these strong interactions and helps to preserve the shape of the central cavity of the JCD.

JCD trimers in solution represent the next step toward longer, self-assembled tubular structures. To analyze their stability, we focused attention exclusively on the collinear docking characterized by a sequence of two PR−SR junctures (see Figure 1). For these trimers, we analyzed distribution functions associated with orientational and spatial order parameters. In panel (a) of Figure 3, we display results for the probability distributions for $Z_i = Z^i_{JCD} - Z^c_{JCD}$, ($i = u, l$) the z-component of the vector joining the centers of mass of the central (c) JCD and those of the upper (u) and lower (l) adjacent units. In panel (b), the plots correspond to distribution involving $\cos\phi_i = \hat{u}_c \cdot \hat{u}_i$, where $\hat{u}_i$ represents a unit vector along the direction of the largest moments of inertia of a JCD which, for β-CDs, is perpendicular to the glycosidic oxygen plane. Although the distributions may differ to a certain extent, for all practical purposes, their corresponding average values and standard deviations are the same, $\langle Z_i \rangle = 10.8 \pm 0.3$ Å (10.8 ± 0.6 Å) and $\langle\cos\phi_i\rangle = 0.98 \pm 0.02$ (0.97 ± 0.03) for the l (u) adjacent units. Moreover, the narrow widths of all distributions provide clear evidence of the robustness of the trimer docking.

It is also of interest of analyze the structure and dynamical characteristics of the trapped water within the central tubular cavity of the JCD trimer. In the bottom panel of Figure 4, we present results for the local oxygen−water density with respect to a system centered at the instantaneous position of the center of mass of the central JCD

$$\rho_O(z) = \frac{1}{\pi R^2} \sum_i H(\mathbf{r}_i)\langle\delta(z^i_O - Z^c_{JCD} - z)\rangle \tag{2}$$

Letters

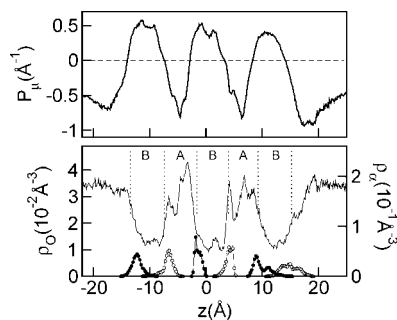*J. Phys. Chem. B, Vol. 113, No. 5, 2009* **1243**

Figure 4. Bottom panel: Site densities within the central cavity of a docked JCD trimer: oxygen water (left axis, solid line); carboxymethyl groups (right axis, open circles); amino groups (right axis, black circles). The vertical dotted lines represent approximate boundaries for solvent-rich ($\mathscr{A}$) and solvent-poor ($\mathscr{B}$) regions (see text). Top panel: Polarization density for trapped water within the central cavity of a docked JCD trimer.

Figure 5. Time correlation function for the population relaxation of trapped water molecules within the tubular structure of a docked JCD trimer.

In the previous equation, z_O^i represents the z-coordinate of the ith water oxygen site, and the characteristic function $H(\mathbf{r}_i)$ is 1 if the ith particle lies within a cylindrical volume of radius $R = 6$ Å, whose axis coincides with $\hat{\mathbf{u}}_c$ and 0 otherwise. As such, sampling at small values of $|z|$ is restricted to those water molecules trapped in the tubular cavity. The curve presents two structureless regions for $|z| \gtrsim 18$ Å, which correspond to bulk water. In between, there is a central portion where the oxygen density presents alternation of solvent-rich ($\mathscr{A}$) and solvent-poor ($\mathscr{B}$) regions. The simultaneous examination of the z dependence of the N (amino) and C (carboxymethyl) site densities (also shown in the figure) is helpful to rationalize this feature. Note that $\mathscr{A}$ segments clearly correlate with the position of the charged rims, whereas $\mathscr{B}$ segments coincide with the three inter-rim monomer cavities. Direct integrations of the density over appropriate limits yield an average population of $\langle N_O^{\mathscr{A}} \rangle \sim 13$ ($\langle N_O^{\mathscr{B}} \rangle \sim 6$) confined water molecules in each region of type $\mathscr{A}(\mathscr{B})$. In passing, we note that our estimate for $\langle N_O^{\mathscr{B}} \rangle$ agrees reasonably well with the results recently reported by Raffaini et al.[23]

Tracing back the origins of the structural stability of the JCD trimer, we looked into the details concerning intermolecular connectivity at the $\mathscr{A}$ joints. In a typical configuration, practically all groups which can act as hydrogen-bond (HB) donors and/or acceptors participate in these bondings, which, in turn, contribute to preserve the overall tubular structure of the trimer. Concerning HB partners, one normally observes not only direct, rim-to-rim bonds of the type $-COO^- \cdots {}^+H_3N-$ but also rim-to-water bonds of the type $-COO^- \cdots H_2O$ and $H_2O \cdots {}^+H_3N-$ and even more complex bridged structures, involving wedged water, of the type $-COO^- \cdots H_2O \cdots {}^+H_3N-$.

The analysis of the polarization structure of the trapped water is also of interest. In the top panel Figure 4, we present results for the polarization distribution

$$P_\mu(z) = \frac{1}{\pi R^2} \sum_i H(\mathbf{r}_i) \langle \delta(z_O^i - Z_{JCD}^c - z) \cos \theta_i \rangle \quad (3)$$

where θ_i is equal to the angle between the dipole of the ith water and the z-axis. Note that the peculiar characteristics of the alternate charge distribution located at the top and bottom rims dictate the polarization response of the confined water molecules. At the crudest level of description, this polarization structure can be casted in terms of a dielectric continuum
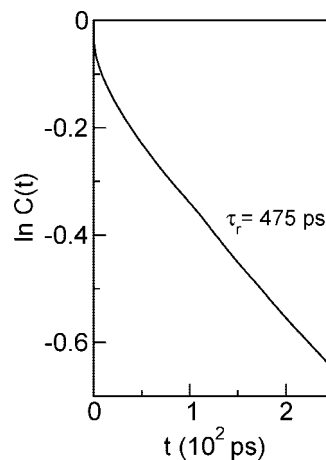
surrounding six charged planar plates of alternating signs, located at the rim positions.

Given the sharp characteristics of the spatial and polarization correlations observed for the confined water molecules, one can also anticipate important modifications in their dynamics. Perhaps the simplest parameter to estimate these effects is τ_r, the average residence time within the central tubular structure. The analysis of long time behavior of the time correlation function for the population relaxation of trapped water, namely, $C(t) = \langle \delta n_i(t) \delta n_i(0) \rangle$, is an adequate route to compute τ_r. In the previous expression, $\delta n_i = n_i - \langle n_i \rangle$ and $n_i(t) = 1$ if particle i is trapped within the tubular cavity at time t and are 0 otherwise. The plot for $C(t)$ is displayed in Figure 5; after an initial ~ 25 ps transient period, the long time portion of the normalized $C(t)$ clearly exhibits a single-exponential decay, with characteristic time scale $\tau_r = 475 \pm 60$ ps. The analysis of an ensemble of trajectories of trapped molecules shows a variety of paths, most notably those in which water molecules enter into the cavity by the outer rims, leaving either through the same rim or at one of the two junctions between adjacent JCDs. Although less frequently, we also encountered diffusive paths that span the complete length of the cylindrical tube, $l \sim 25-30$ Å. To assess the extent of the overall retardation experimented by the diffusional motion of the trapped water molecules, one can compare τ_r with two related time scales, (i) on the one hand, the residence time $\tau_r^{sing} \sim 75$ ps reported by Rodriguez et al.[24] for a single, nonfunctionalized β-CD and (ii) on the other hand, the time that is required for the diffusion of a bulk water molecule to travel a distance comparable to the typical length of a trapped one-dimensional path, say, $l/2$, $\tau \sim (l/2)^2/2D_w \sim 150$ ps. In the previous expression, $D_w = 0.62$ Å^2 ps^{-1} stands for the diffusion coefficient of the TIP3P water model[10,25] implemented in this study.

Summarizing, we have analyzed the stability of JCD dimers and trimers in solution. From energetic grounds, the JCD dimer is $\sim 3-4$ times more stable than nonfunctionalized CD ones. Face-to-face docking in trimers yields tubular structures which exhibit minimal distortions in their spatial and orientational distributions. Spatial and polarization local densities of trapped water within the tubular structure present strong fluctuations which are dictated by the charge density at the rims. The latter correlations also promote important retardations in the intratube water diffusion. The overall picture that emerges from this body of information corroborates the role of JCDs as building blocks of aqueous nanotubes in solution.

References and Notes

(1) For comprehensive information about cyclodextrins, see the special issue corresponding to *Chem. Rev.* **1998**, *98*.

(2) Hamelin, B.; Jullien, L.; Guillo, F.; Lehn, J.-M.; Jardy, A.; De Robertis, L.; Driguez, H. *J. Phys. Chem.* **1995**, *99*, 17877.

(3) Shiwinté, P.; Holohan, A.; Darcy, R.; O'Keefe, F. *J. Inclusion Phenom. Macrocyclic Chem.* **1999**, *35*, 657.

(4) Sallas, F.; Darcy, R. *Eur. J. Org. Chem.* **2008**, 957.

(5) Parrot-Lopez, H.; Ling, C.-C.; Zhang, P.; Baszkin, A.; Albrecht, G.; de Rango, C.; Coleman, A. W. *J. Am. Chem. Soc.* **1992**, *114*, 5479.

(6) Bart, J. R.; Darcy, R.; Mazzaglia, A.; Nolan, D.; Gaffney, K. *Chem. Commun.* **2001**, 827.

(7) Dehez, F.; Tarek, M.; Chipot, C. *J. Phys. Chem. B* **2007**, *111*, 10633.

(8) Phillips, J. C.; Braun, R.; Wang, W.; Gumbart, J.; Takkhorshid, E.; Villa, E.; Chipot, C.; Skeel, R. D.; Kalé, L. V.; Shulten, K. *J. Comput. Chem.* **2005**, *26*, 1781.

(9) Mackerell, J. A. D.; Bashford, D.; Bellott, M.; Dunbrack, J. R. L.; Evanseck, J. D.; Field, M. J.; Fischer, S.; Gao, J.; Guo, H.; Ha, S.; Joseph-McCarthy, D.; Kuchnir, L.; Kuczera, K.; Lau, F. T. K.; Mattos, C.; Michnick, S.; Ngo, T.; Nguyen, D. T.; Prodhom, B.; Reiher, W. E.; Roux, B.; Schlenkrich, M.; Smith, J. C.; Stote, R.; Straub, J.; Watanabe, W.; Wiórkiewicz-Kuczera, J.; Yin, D.; Karplus, M. *J. Phys. Chem. B* **1998**, *102*, 3586.

(10) Jorgensen, W. L.; Chandrasekhar, J.; Madura, J. D. *J. Chem. Phys.* **1983**, *79*, 926.

(11) Darden, T. A.; York, D. M.; Pedersen, L. G. *J. Chem. Phys.* **1993**, *98*, 10089.

(12) Essmann, U.; Perera, L.; Berkowitz, M. L.; Darden, T. A.; Lee, H.; Pedersen, L. G. *J. Chem. Phys.* **1995**, *103*, 8577.

(13) Available at: Hetero-compound Information Centre-Uppsala. http://xray.bmc.uu.se/hicup/ACX/index.html.

(14) Hwang, H.; Schatz, G. C.; Ratner, M. A. *J. Phys. Chem. B* **2006**, *110*, 26448.

(15) Yu, Y.; Chipot, C.; Cai, W.; Shao, X. *J. Phys. Chem. B* **2006**, *110*, 6372.

(16) Yu, Y.; Chipot, C.; Sun, T.; Shao, X. *J. Phys. Chem. B* **2008**, *112*, 5268.

(17) Darve, E.; Pohorille, A. *J. Chem. Phys.* **2001**, *115*, 9169.

(18) Hénin, J.; Chipot, C. *J. Chem. Phys.* **2004**, *121*, 2904.

(19) Rodriguez-Gomez, D.; Darve, E.; Pohorille, A. *J. Chem. Phys.* **2004**, *120*, 3563.

(20) Bonnet, P.; Jaime, C.; Morin-Alloy, L. *J. Org. Chem.* **2002**, *67*, 8602.

(21) Berkowitz, M.; Karim, O. A.; Mccammon, A. J.; Rossky, P. J. *Chem. Phys. Lett.* **1984**, *105*, 577.

(22) Ciccotti, G.; Ferrario, M.; Hynes, J. T.; Kapral, R. *J. Chem. Phys.* **1990**, *93*, 7137.

(23) Raffaini, G.; Ganazzoli, F. *Chem. Phys.* **2007**, *333*, 128.

(24) Rodriguez, J.; Rico, D. H.; Domenianni, L.; Laria, D. *J. Phys. Chem. B* **2008**, *112*, 7522.

(25) Pekka, M.; Nilsson, L. *J. Phys. Chem. A* **2001**, *105*, 9954.